Contact conductance governs metallicity in conducting metal oxide nanocrystal films

Corey M. Staller[1‡], Stephen L. Gibbs[1‡], Xing Yee Gan[1], Jay T. Bender[1], Karalee Jarvis[2], Gary K. Ong[1], Delia J. Milliron[1]*

[1]McKetta Department of Chemical Engineering, University of Texas at Austin, Austin, Texas 78712, USA.
[2]Texas Materials Institute, University of Texas at Austin, Austin, Texas 78712, USA
‡These authors contributed equally.
*Corresponding author. Email: milliron@che.utexas.edu

Abstract: Although colloidal nanoparticles hold promise for fabricating electronic components, the properties of nanoparticle-derived materials can be unpredictable. Materials made from metallic nanocrystals exhibit a variety of transport behavior ranging from insulators, with inter-nanocrystal contacts acting as electron transport bottlenecks, to conventional metals, where phonon scattering limits electron mobility. The insulator-metal transition (IMT) in nanocrystal films is thought to be determined by contact conductance. Meanwhile, criteria are lacking to predict the characteristic transport behavior of metallic nanocrystal films beyond this threshold. Using a library of transparent conducting tin-doped indium oxide nanocrystal films with varied electron concentration, size, and contact area, we assess the IMT as it depends on contact conductance and show how contact conductance is also key to predicting the temperature-dependence of conductivity in metallic films. The results establish a phase diagram for electron transport behavior that can guide the creation of metallic conducting materials from nanocrystal building blocks.

Keywords: Transparent conductor, insulator-metal transition, doped semiconductor nanocrystals, solution processing, atomic layer deposition, indium tin oxide, variable temperature conductivity

Main text: Metallic nanoparticles, including elemental metals and doped semiconductors, hold promise as solution-processible building blocks to prepare conducting materials, from metallic interconnects to transparent conducting films and electrocatalytic aerogels.[1–7] But such materials exhibit wide-ranging transport properties and often their conductivity is thermally activated, implying they are in fact insulators.[8–13] Unless the nanocrystals are fused into bulk metals, for example by thermal annealing, conventional metallic behavior has rarely been observed.[2,9] In such cases, conductivity decreases as temperature increases since phonon scattering limits the electron mobility. Between these two limits, nanostructured materials may be metallic, meaning their conductivity approaches a finite, non-zero value in the low-temperature limit, but still have an unusual *negative* thermal coefficient of resistivity (TCR).[9,14–16] Although strengthening electronic coupling, by using solution- or vapor-phase deposition to fill the spaces between metal oxide nanocrystals[2,9,11] or replacing long insulating ligands with shorter ones,[6,17,18] is known to increase conductivity, criteria determining the temperature-dependent transport behavior remain the subject of intense investigation.[8–11]

Establishing clear criteria to predict electronic properties has been challenging in part due to limitations in tuning physical parameters that determine conductivity, such as nanocrystal size,

electron concentration, and the strength of electronic coupling between nanocrystals. In bulk materials, the electron concentration predicts the transition from insulating to metallic, as described by the Mott criterion.[19] Materials fabricated from metallic nanoparticles, whether classical metals like gold and silver or semiconductors doped to exceed the Mott criterion, can exhibit the full range of transport properties. In films of metallic nanocrystals, the insulator-metal transition (IMT) has been proposed to occur when the contact conductance (g_c) reaches the quantum conductance ($e^2/\pi\hbar$).[8,20] To relate this criterion to experimentally controllable parameters, it is helpful to recast it in terms of the size of the contacts and the electron concentration. Specifically, the contacts must be larger than the characteristic length scale of the conduction electrons to produce a metal, as shown in Eqn. 1, where k_F is the Fermi wavenumber, which increases with electron concentration (n) as $n^{1/3}$, and r_c is the contact radius.[8]

$$k_F r_c \geq 2 \qquad (1)$$

Experimental tests of this prediction in films of doped silicon or zinc oxide nanocrystals have found qualitative agreement,[8–11] but these tests have been limited by the challenges of tuning n over a wide range and of controllably varying nanocrystal size (r_{NC}) and r_c. Meanwhile, a criterion describing necessary conditions for nanocrystal films to exhibit conventional metallic behavior, with a positive TCR, has remained unspecified.

Here, by observing the temperature-dependent conductivity of a library of 54 tin-doped indium oxide (ITO) nanocrystal films with varied n, r_{NC}, and r_c, we show that contact conductance governs both the IMT and the crossover to conventional metallic behavior near room temperature. Encompassing a wider range of conductivity and g_c, and controlling nanocrystal size more precisely than previous studies, our results indicate that the absolute value of g_c, as it compares to the quantum conductance, controls the IMT, further validating Eqn 1. The conventional metal crossover, however, occurs when g_c reaches the nanocrystal conductance, g_{NC}, which varies from sample to sample depending on nanocrystal size and dopant concentration. These two criteria together establish a phase diagram that quantitatively describes electron transport and can broadly enable the design and fabrication of metallic conducting materials from nanocrystal building blocks.

Preparation and characterization of nanocrystal films

In solution deposited films of ITO nanocrystals, we removed insulating ligands to leave nanocrystals in direct contact, then tuned r_c by conformal deposition of indium oxide to control the neck between adjacent nanocrystals. Nanocrystals are synthesized with diameters from 5 to 20 nm with low dispersity by solution-phase synthesis during which Sn dopants are incorporated uniformly throughout the nanocrystals up to 5 at% (Fig. 1A and S1).[21] Organic ligands that facilitate solvent casting of uniform thin films are then chemically stripped, leaving the bare nanocrystals in direct contact.[12,22] Following a strategy used previously for ZnO nanocrystal films,[9,11] the spaces between the nanocrystals are in-filled by atomic layer deposition (ALD), first with indium oxide to conformally coat the interior surfaces and variably increase r_c, then with aluminum oxide to eliminate surface depletion layers that would diminish g_c (Fig. 1B-E).[12,13] Fabrication of the films, which are highly transparent, is further described in the Supporting Information, with a photo and additional electron micrographs in Figs. S2-6.
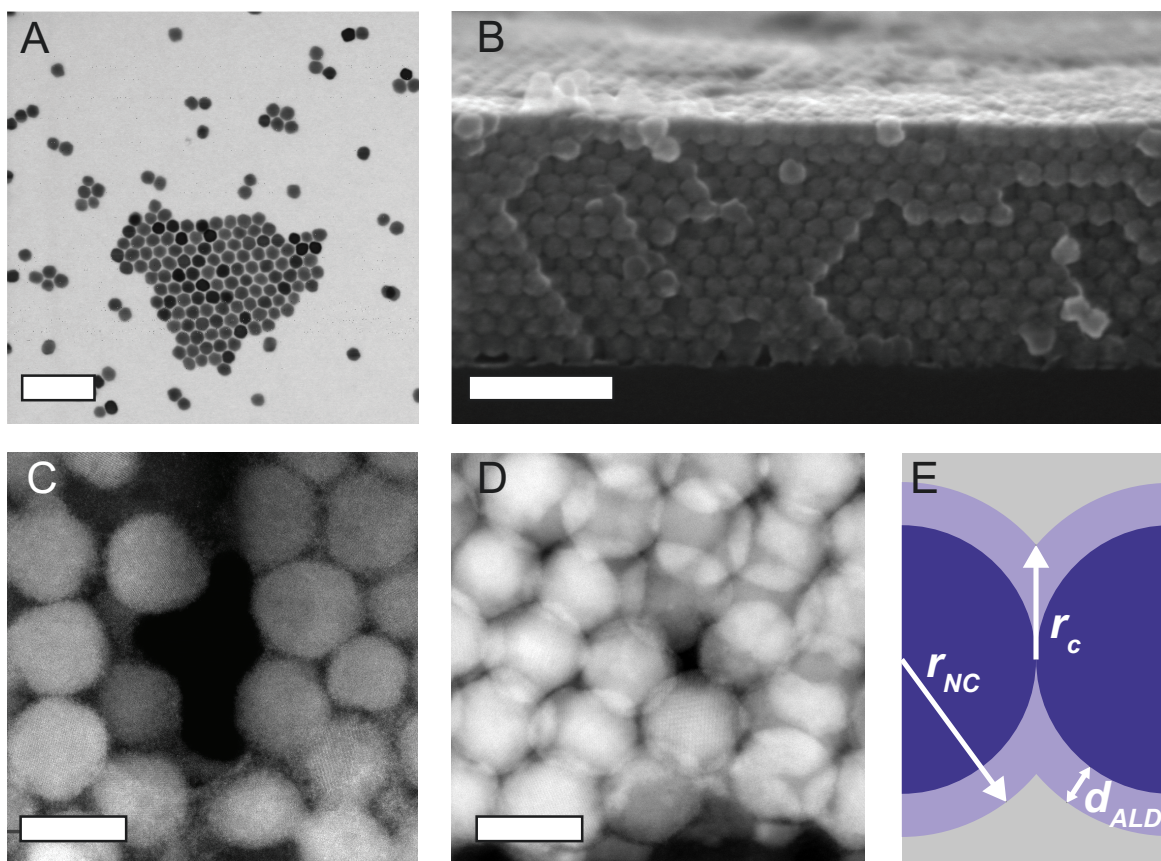
Figure 1. Electron microscopy of nanocrystal films. (**A**) Bright-field scanning transmission electron microscopy (STEM) of 20 nm 3 at% Sn ITO nanocrystals. (**B**) Cross-sectional scanning electron microscopy of a film of 20 nm In_2O_3 nanocrystals after indium oxide ALD. Scale bars are 100 nm. (**C**, **D**) High-resolution cross-sectional STEM high-angle annular dark field images of finished films with no indium oxide ALD (**C**) and 40 cycles of indium oxide ALD (**D**), with scale bars of 20 nm. (**E**) Indium oxide ALD (light blue) expands both the nanocrystals (dark blue) and their contact radius with aluminum oxide (gray) filling the remaining pore volume.

Evaluation of transport behavior

The transport behavior of each of 54 films, made from 9 different synthetic batches of nanocrystals with varied cycles of ALD indium oxide, was ascertained by examining the temperature dependence of the conductivity from above room temperature down to a few degrees Kelvin (Figs. 2, S7-9). Larger nanocrystals, higher dopant concentration, and increasing indium oxide ALD thickness all tend toward metallicity, but none of these factors is independently predictive of the transport behavior. To categorize samples as metals or insulators, it was important to examine the trajectory of the conductivity at low temperatures to determine whether the zero-temperature limit is nonzero. This assessment is most readily accomplished with a Zabrodskii analysis of the temperature dependent conductivity (σ), plotting $ln\,W$ vs $ln\,T$ where $W = d\,ln\,\sigma\,/d\,ln\,T$.[23] Insulators have a negative slope on a Zabrodskii plot and their thermally activated conductivity could be fit over a broad temperature range to the Efros-

Shklovskii variable-range hopping (ES-VRH) model with a Gaussian dispersion of energy levels (Figs. 2A, S10), similar to many nanocrystal films reported previously.[8–12,24–26] The approximately -0.8 exponent in the temperature dependence exhibited here is a result of temperature dependent heat capacity of ITO, as described previously.[12] Adding indium oxide by ALD increases r_c and the Zabrodskii slopes at low temperature vanish, then become positive, suggesting a finite resistivity in the zero-temperature limit and signaling the IMT threshold has been crossed (Fig. 2B). To assess the metallicity of each sample, we performed Zabrodskii analysis on all 54 temperature-dependent conductivity curves (Fig. S9).
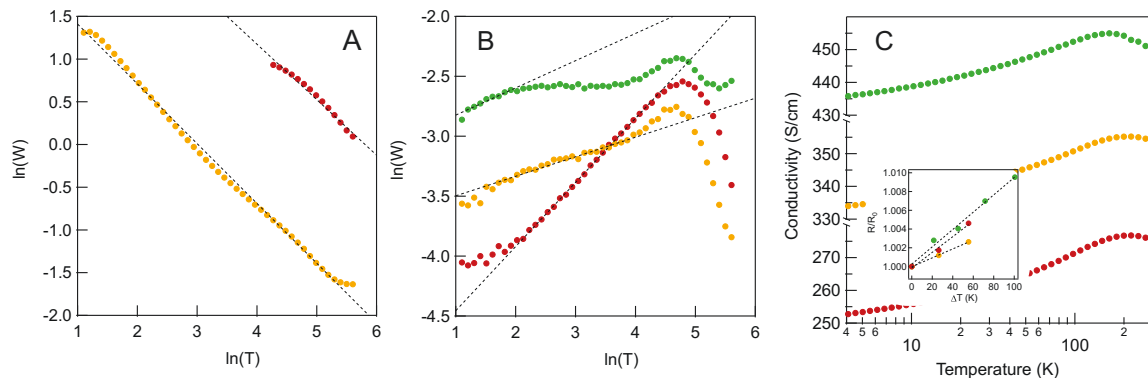

Figure 2. Electron transport behavior determined by variable temperature conductivity.
(**A**) Zabrodskii plots of insulators with negative slopes, indicating divergent resistivity approaching zero Kelvin. (**B**) Zabrodskii plots of metals with positive slopes, indicating finite conductivity in the zero-temperature limit. Lines are guides to the eye for slope in the low temperature regime. (**C**) Conventional metallic behavior is observed around room temperature in some samples. Data are for undoped, 5 nm nanocrystals (red) with 0, 8, or 20 cycles of indium oxide ALD, for 5 at% Sn, 15 nm nanocrystals (yellow) with 0, 6, or 30 cycles, and for 5 at% Sn, 20 nm nanocrystals (green) with 8 or 40 cycles.

However, the temperature-dependence of the conductivity varied for samples found to be metals by analysis of their low temperature behavior. Like other ALD in-filled ZnO and ITO nanocrystal films,[9–12] some samples exhibit negative TCR at all temperatures and are classified as unconventional metals. Their temperature-dependent conductivity can be fit to granular metal or Fermi liquid models, or both in different temperature ranges (Fig. S10). Finally, in some samples a crossover to positive TCR around and above room temperature occurs (Fig. 2C). These samples are classified as conventional metals. A single nanocrystal composition (e.g., 5 at% Sn, 15 nm diameter) can produce films in all three electron transport regimes, depending on the extent of indium oxide ALD (Fig. 2A-C, yellow). The electron transport models are fully described and fit parameters reported in the Supporting Information (Fig. S10 and Tables S1-4).

Assessing criteria for electron transport behavior

To assess the IMT criterion and discover conditions leading to conventional metallic behavior in ITO nanocrystal films, the physical parameters n, r_c, and r_{NC} were determined for each sample. The electron mean free path and initial electron concentration, n_0, before ALD coating were determined by fitting localized surface plasmon resonance (LSPR) absorption spectra of solvent-dispersed nanocrystals (Fig. S11 and Table S5).[27] This approach avoids the complication of

spectral shifts and broadening induced by LSPR-LSPR coupling in nanocrystal films.[2,22,28,29] A tunneling or b-contact model was used to find r_c for samples with no indium oxide ALD coating, while for samples with ALD-enhanced contact area we calculated the effective r_c from g_c values found by analysis of film conductivity (see below). Contact conductance may be related to r_c via the Sharvin equation, which is suitable for contacts small compared to the mean free path:[30]

$$g_c = \frac{k_F^2 r_c^2}{4} \qquad (2)$$

We model the film as a random resistor network,[26] with each resistor comprising the resistance of a nanocrystal and the contact resistance g_c^{-1}, in series.[11] Although this analysis assumes a single, uniform value for g_c, heterogeneity in the contacts is expected only to influence the approach to the IMT,[18] not the transition threshold itself.[20] The electronic properties (n and the electron mean free path) extracted by fitting LSPR spectra[27] are used to calculate the conductance of a nanocrystal, g_{NC}, and so determine g_c and r_c for each sample. In this analysis, the thickness of the indium oxide added by ALD, d_{ALD}, is considered a single parameter that constrains the relationship between r_c and r_{NC} geometrically (Fig. 1E). The electron concentration used for analysis was reduced from n_0 in proportion to the increasing nanocrystal volume and the electron mean free path was adjusted to account for surface scattering, depending on r_c and r_{NC} for each sample.[31] Because all samples are fully in-filled by alumina ALD, we know from prior work carried out on similarly prepared ITO nanocrystal films[12] that depletion layers vanish, making the energy band profiles and carrier profiles uniform throughout the nanocrystal. In that study, depletion layer changes brought about by varying the radial placement of dopants strongly influenced conductivity in films without any ALD post-processing. But in-filling with alumina ALD enhanced conductivity of all films and eliminated any influence of dopant placement, suggesting the removal of depletion effects. Here, electron concentrations determined by Hall effect measurements were found to be in good approximate agreement with the optically derived values for metallic films, where Hall analysis is expected to be most reliable (Fig. S12), further supporting our approach to estimating n. Further information on establishing these physical parameters is found in the Supporting Information.

To evaluate the success of the Eqn.1 in predicting the IMT, we considered all samples and found reasonable agreement (Fig. 3). Two samples could not be readily categorized by Zabrodskii analysis (Fig. S9). Otherwise, only one sample, with g_c slightly below the quantum conductance, was found to violate the predicted threshold. The cross-validation of electron concentrations by optical and Hall effect analysis, as well as the highly uniform size and organization of our nanocrystals, makes this assessment a notable extension to previous experiments aimed at testing Eqn. 1.[8–11] Our samples also span four orders of magnitude in conductivity and five orders of magnitude in g_c, with many more samples above the IMT than in previous studies.
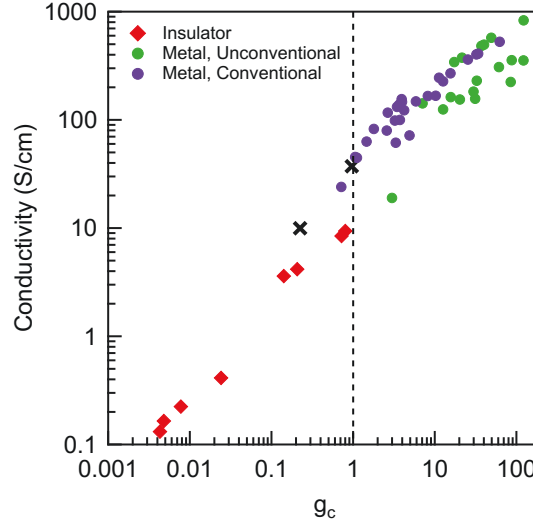
Figure 3. Assessment of IMT criterion. Room temperature conductivity of ITO nanocrystal films with the observed electron transport behavior indicated by the symbol for each data point. Two samples that could not be classified based on Zabrodskii analysis are shown as **x** . The g_c axis is in units of the quantum conductance and the vertical dashed line indicates the predicted IMT.

Many of the metal samples exhibit conventional behavior (positive TCR) around room temperature, but Fig. 3 makes it clear that neither the conductivity nor g_c can predict this behavior. For instance, we found metals with room temperature conductivity as high as 500 S cm^{-1} to have unconventional temperature dependence and metals with room temperature conductivity well below 100 S cm^{-1} to be conventional metals. It was suggested previously that metals will cease to behave as granular conductors when g_c is no longer less than g_{NC}, which we therefore hypothesized may determine the crossover to conventional metallic conductivity in our ITO nanocrystal films. Indeed, with near perfect agreement, samples with

$$g_c \geq g_{NC} \qquad (3)$$

have positive TCR near room temperature (Fig. 4A), meaning their conductivity is limited by the conductivity of the nanocrystals themselves, rather than the contacts.
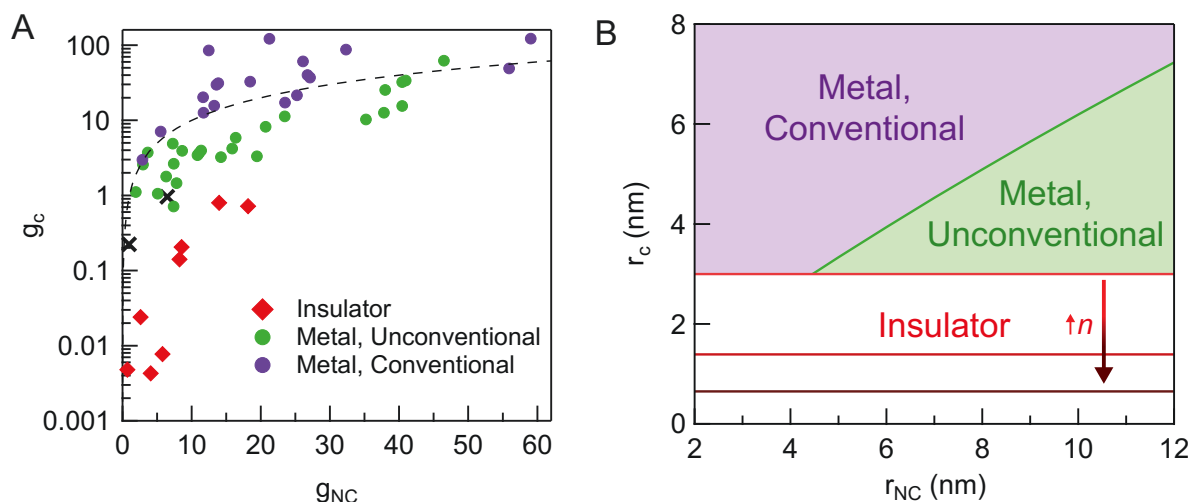
Figure 4. Electron transport mechanism phase diagram. (**A**) Good agreement with Eqn. 3 to predict conventional metal behavior near room temperature. (**B**) The two thresholds (Eqns. 1 and 3) determine the boundaries on the electron transport mechanism phase diagram, which are plotted for nanocrystals of $n = 10^{25}$, 10^{26}, and 10^{27} m^{-3}. Note that as n increases, the IMT boundary shifts downward while the crossover to conventional metal behavior does not change. Again, two samples that could not be classified based on Zabrodskii analysis are shown as x.

Discussion

The two criteria (Eqns. 1 and 3), when expressed in terms of physical characteristics of the nanocrystal films (n, r_c, and r_{NC}), establish boundaries on an electron transport phase diagram (Fig. 4B). The crossover to conventional metallic behavior is independent of n since it depends only on the ratio of g_c and g_{NC}, which scale identically with n. In contrast, the IMT depends strongly on n. Regardless of nanocrystal size, the required contact area to cross the IMT is reduced at higher n, recalling the analysis by Chen, et al.[8]

Variable temperature conductivity measurements of films of ITO nanocrystals varying in size, electron concentration, and contact radius indicate the derived transition and crossover criteria are robust. We have established the electron transport phase for a prototypical doped metal oxide, which has the potential to be applied for transparent contacts in optoelectronic devices, while the derived results are also expected to apply to other doped semiconductors, including doped silicon nanocrystals,[8] ZnO nanocrystals,[9–11] or metal chalcogenide nanocrystals doped remotely.[3,4] The criteria also make plain the importance of the contact conductance in governing transport, suggesting novel strategies for design and fabrication of metallic nanocrystal films. For example, highly conductive contacts could be created by introducing distinct, conductive materials at the contact points[32] or by using faceted nanocrystals that pack face-to-face during deposition to enhance contact area.[2] More broadly, these guidelines could enable deliberate tuning of nanocrystal films, networks, and assemblies to meet the design criteria for specific electronic or electrochemical applications.

Author information

Corresponding author
E-mail: milliron@che.utexas.edu
Telephone: (512)232-5702
Notes: The authors declare no competing financial interest.

Associated content

Supporting information: The Supporting Information is available free of charge on the ACS Publications website at DOI:XXX. Supplementary text describing materials and methods and explaining, in detail, the formulation required to fit data and calculate resulting parameters. Figures S1-S13 and Tables S1-S5 providing data supporting the analysis and discussion in the main text, including additional electron microscopy, optical spectroscopy, temperature-dependent conductivity, Hall effect, and ellipsometric porosimetry data.

Acknowledgements

Author contributions

Conceptualization, sample fabrication, and data acquisition were carried out by CMS, GKO, XYG, JTB, and KJ. Analysis and visualization were performed by CMS and SLG. Writing was completed by CMS, SLG, and DJM with input from all authors.

References

(1)   Crockett, B. M.; Jansons, A. W.; Koskela, K. M.; Sharps, M. C.; Johnson, D. W.; Hutchison, J. E. Influence of Nanocrystal Size on the Optoelectronic Properties of Thin, Solution-Cast Sn-Doped In$_2$O$_3$ Films. *Chem. Mater.* **2019**, *31*, 3370–3380.

(2)   Kim, B. H.; Staller, C. M.; Cho, S. H.; Heo, S.; Garrison, C. E.; Kim, J.; Milliron, D. J. High Mobility in Nanocrystal-Based Transparent Conducting Oxide Thin Films. *ACS Nano* **2018**, *12*, 3200–3208.

(3)   Yu, D.; Wang, C.; Guyot-Sionnest, P. N-Type Conducting CdSe Nanocrystal Solids. *Science* **2003**, *300*, 1277–1280.

(4)   Talapin, D. V.; Murray, C. B. PbSe Nanocrystal Solids for N- and p-Channel Thin Film Field-Effect Transistors. *Science* **2005**, *310*, 86–89.

(5)   You, J.; Meng, L.; Song, T.-B.; Guo, T.-F.; Yang, Y. (Michael); Chang, W.-H.; Hong, Z.; Chen, H.; Zhou, H.; Chen, Q.; Liu, Y.; De Marco, N.; Yang, Y. Improved Air Stability of

Perovskite Solar Cells via Solution-Processed Metal Oxide Transport Layers. *Nat. Nanotechnol.* **2016**, *11*, 75–81.

(6)   Coropceanu, I.; Janke, E. M.; Portner, J.; Haubold, D.; Nguyen, T. D.; Das, A.; Tanner, C. P. N.; Utterback, J. K.; Teitelbaum, S. W.; Hudson, ˌ Margaret H.; Sarma, N. A.; Hinkle, A. M.; Tassone, C. J.; Eychmüller, A.; Limmer, D. T.; Olvera de la Cruz, M.; Ginsberg, N. S.; Talapin, D. V. Self-Assembly of Nanocrystals into Strongly Electronically Coupled All-Inorganic Supercrystals. *Science* **2022**, *375*, 1422–1426.

(7)   Liu, W.; Herrmann, A.-K.; Bigall, N. C.; Rodriguez, P.; Wen, D.; Oezaslan, M.; Schmidt, T. J.; Gaponik, N.; Eychmüller, A. Noble Metal Aerogels—Synthesis, Characterization, and Application as Electrocatalysts. *Acc. Chem. Res.* **2015**, *48*, 154–162.

(8)   Chen, T.; Reich, K. V.; Kramer, N. J.; Fu, H.; Kortshagen, U. R.; Shklovskii, B. I. Metal–Insulator Transition in Films of Doped Semiconductor Nanocrystals. *Nat. Mater.* **2016**, *15*, 299–303.

(9)   Greenberg, B. L.; Robinson, Z. L.; Ayino, Y.; Held, J. T.; Peterson, T. A.; Mkhoyan, K. A.; Pribiag, V. S.; Aydil, E. S.; Kortshagen, U. R. Metal-Insulator Transition in a Semiconductor Nanocrystal Network. *Sci. Adv.* **2019**, *5*, eaaw1462.

(10)   Greenberg, B. L.; Robinson, Z. L.; Reich, K. V.; Gorynski, C.; Voigt, B. N.; Francis, L. F.; Shklovskii, B. I.; Aydil, E. S.; Kortshagen, U. R. ZnO Nanocrystal Networks Near the Insulator–Metal Transition: Tuning Contact Radius and Electron Density with Intense Pulsed Light. *Nano Lett.* **2017**, *17*, 4634–4642.

(11)   Lanigan, D.; Thimsen, E. Contact Radius and the Insulator–Metal Transition in Films Comprised of Touching Semiconductor Nanocrystals. *ACS Nano* **2016**, *10*, 6744–6752.

(12)   Staller, C. M.; Robinson, Z. L.; Agrawal, A.; Gibbs, S. L.; Greenberg, B. L.; Lounis, S. D.; Kortshagen, U. R.; Milliron, D. J. Tuning Nanocrystal Surface Depletion by Controlling Dopant Distribution as a Route Toward Enhanced Film Conductivity. *Nano Lett.* **2018**, *18*, 2870–2878.

(13)   Ephraim, J.; Lanigan, D.; Staller, C.; Milliron, D. J.; Thimsen, E. Transparent Conductive Oxide Nanocrystals Coated with Insulators by Atomic Layer Deposition. *Chem. Mater.* **2016**, *28*, 5549–5553.

(14)   Bogdanovich, S.; Sarachik, M. P.; Bhatt, R. N. Scaling of the Conductivity with Temperature and Uniaxial Stress in Si:B at the Metal-Insulator Transition. *Phys. Rev. Lett.* **1999**, *82*, 137–140.

(15)   Beloborodov, I. S.; Lopatin, A. V.; Vinokur, V. M. Universal Description of Granular Metals at Low Temperatures: Granular Fermi Liquid. *Phys. Rev. B* **2004**, *70*, 205120.

(16)   Waffenschmidt, S.; Pfleiderer, C.; Löhneysen, H. v. Critical Behavior of the Conductivity of Si:P at the Metal-Insulator Transition under Uniaxial Stress. *Phys. Rev. Lett.* **1999**, *83*, 3005–3008.

(17)   Fafarman, A. T.; Hong, S.-H.; Caglayan, H.; Ye, X.; Diroll, B. T.; Paik, T.; Engheta, N.; Murray, C. B.; Kagan, C. R. Chemically Tailored Dielectric-to-Metal Transition for the Design of Metamaterials from Nanoimprinted Colloidal Nanocrystals. *Nano Lett.* **2013**, *13*, 350–357.

(18)   Müller, K.-H.; Wei, G.; Raguse, B.; Myers, J. Three-Dimensional Percolation Effect on Electrical Conductivity in Films of Metal Nanoparticles Linked by Organic Molecules. *Phys. Rev. B* **2003**, *68*, 155407.

(19)   Mott, N. F. Metal-Insulator Transition. *Rev. Mod. Phys.* **1968**, *40*, 677–683.

(20) Beloborodov, I. S.; Lopatin, A. V.; Vinokur, V. M.; Efetov, K. B. Granular Electronic Systems. *Rev. Mod. Phys.* **2007**, *79*, 469–518.

(21) Jansons, A. W.; Hutchison, J. E. Continuous Growth of Metal Oxide Nanocrystals: Enhanced Control of Nanocrystal Size and Radial Dopant Distribution. *ACS Nano* **2016**, *10*, 6942–6951.

(22) Garcia, G.; Buonsanti, R.; Runnerstrom, E. L.; Mendelsberg, R. J.; Llordes, A.; Anders, A.; Richardson, T. J.; Milliron, D. J. Dynamically Modulating the Surface Plasmon Resonance of Doped Semiconductor Nanocrystals. *Nano Lett.* **2011**, *11*, 4415–4420.

(23) Zabrodskii, A. G. The Coulomb Gap: The View of an Experimenter. *Philos. Mag. B* **2001**, *81*, 1131–1151.

(24) Houtepen, A. J.; Kockmann, D.; Vanmaekelbergh, D. Reappraisal of Variable-Range Hopping in Quantum-Dot Solids. *Nano Lett.* **2008**, *8*, 3516–3520.

(25) Thimsen, E.; Johnson, M.; Zhang, X.; Wagner, A. J.; Mkhoyan, K. A.; Kortshagen, U. R.; Aydil, E. S. High Electron Mobility in Thin Films Formed via Supersonic Impact Deposition of Nanocrystals Synthesized in Nonthermal Plasmas. *Nat. Commun.* **2014**, *5*, 5822.

(26) Shklovskiǐ, B. I.; Éfros, A. L. Percolation Theory and Conductivity of Strongly Inhomogeneous Media. *Sov. Phys. Uspekhi* **1975**, *18*, 845.

(27) Gibbs, S. L.; Staller, C. M.; Agrawal, A.; Johns, R. W.; Saez Cabezas, C. A.; Milliron, D. J. Intrinsic Optical and Electronic Properties from Quantitative Analysis of Plasmonic Semiconductor Nanocrystal Ensemble Optical Extinction. *J. Phys. Chem. C* **2020**, *124*, 24351–24360.

(28) Agrawal, A.; Cho, S. H.; Zandi, O.; Ghosh, S.; Johns, R. W.; Milliron, D. J. Localized Surface Plasmon Resonance in Semiconductor Nanocrystals. *Chem. Rev.* **2018**, *118*, 3121–3207.

(29) Mendelsberg, R. J.; Garcia, G.; Milliron, D. J. Extracting Reliable Electronic Properties from Transmission Spectra of Indium Tin Oxide Thin Films and Nanocrystal Films by Careful Application of the Drude Theory. *J. Appl. Phys.* **2012**, *111*, 063515.

(30) Sharvin, Yu. V. A Possible Method for Studying Fermi Surfaces. *Sov. J. Exp. Theor. Phys.* **1965**, *21*, 655.

(31) Staller, C. M.; Gibbs, S. L.; Saez Cabezas, C. A.; Milliron, D. J. Quantitative Analysis of Extinction Coefficients of Tin-Doped Indium Oxide Nanocrystal Ensembles. *Nano Lett.* **2019**, *19*, 8149–8154.

(32) Tangirala, R.; Baker, J. L.; Alivisatos, A. P.; Milliron, D. J. Modular Inorganic Nanocomposites by Conversion of Nanocrystal Superlattices. *Angew. Chem. Int. Ed.* **2010**, *49*, 2878–2882.

For TOC only: